

One-shot domain adaptation in video-based assessment of surgical skills

Erim Yanik^{1*}, Steven Schwartzberg², Gene Yang², Xavier Intes³, Jack Norfleet⁴, Matthew Hackett⁴, and Suvrana De¹

¹ College of Engineering, Florida A&M University and The Florida State University, USA

² School of Medicine and Biomedical Sciences, University at Buffalo, USA

³ Biomedical Engineering Department, Rensselaer Polytechnic Institute, USA

⁴ U.S. Army Combat Capabilities Development Command Soldier Center STTC, USA

Deep Learning (DL) has achieved automatic and objective assessment of surgical skills. However, the applicability of DL models is often hampered by their substantial data requirements and confinement to specific training domains. This prevents them from transitioning to new tasks with scarce data. Therefore, domain adaptation emerges as a critical element for the practical implementation of DL in real-world scenarios. Herein, we introduce A-VBANet, a novel meta-learning model capable of delivering domain-agnostic surgical skill classification via one-shot learning. A-VBANet has been rigorously developed and tested on five diverse laparoscopic and robotic surgical simulators. Furthermore, we extend its validation to operating room (OR) videos of laparoscopic cholecystectomy. Our model successfully adapts with accuracies up to 99.5% in one-shot and 99.9% in few-shot settings for simulated tasks and 89.7% for laparoscopic cholecystectomy. This research marks the first instance of a domain-agnostic methodology for surgical skill assessment, paving the way for more precise and accessible training evaluation across diverse high-stakes environments such as real-life surgery where data is scarce.

Introduction

There is growing interest in applying deep learning (DL) methodologies for surgical skill assessment^{1,2}. While DL models^{2–17} have shown potential in facilitating real-time, objective skill evaluation, their effectiveness is contingent upon substantial, procedure-specific data availability. The scarcity of such data^{18–21}, coupled with the high costs² and extensive time required for data collection and annotation in real surgical environments²², limits the current DL model’s broader utility. Generalizing these models to diverse surgical tasks – or domains – necessitates labor-intensive methodologies like transfer learning^{23,24}, a daunting task given the vast diversity of surgical procedures. Therefore, a major hurdle for the wide dissemination of DL models in clinical practice is their ability to adapt to new surgical procedures with limited data availability robustly.

To overcome this limitation, we propose the Adaptive Video-Based Assessment Network (A-VBANet), a domain-agnostic DL model designed for surgical skill assessment using video streams. Fig. 1 details our approach. A-VBANet leverages few-(one-)shot^{24–28} meta-learning^{24,29–34} techniques, which involve training models to quickly adapt to new tasks with minimal data, to demonstrate adaptability across a variety of settings, including five physical simulators and laparoscopic cholecystectomy procedures in the operating room (OR). To our knowledge, the integration of meta-learning in surgical skill assessment has not been explored in existing literature, with the closest study focusing on adaptive tool detection²⁸. This renders our pipeline the first in the field. A-VBANet holds promise for widespread application in surgical skill assessment and credentialing, addressing the critical need for adaptable and efficient skill evaluation in diverse surgical environments, especially cohorts with limited data.

Methods

Metaset generation. *Cohorts 1-2: Laparoscopic pattern cutting and suturing.* Collected in collaboration with the University at Buffalo, pattern cutting and suturing are subtasks of the Fundamentals of

Laparoscopic Surgery (FLS) program, a prerequisite for board certification³⁵. For both, Institutional Review Board (IRB) approval was sought at Rensselaer Polytechnic Institute and the University at Buffalo. Further, written informed consent was collected from each subject.

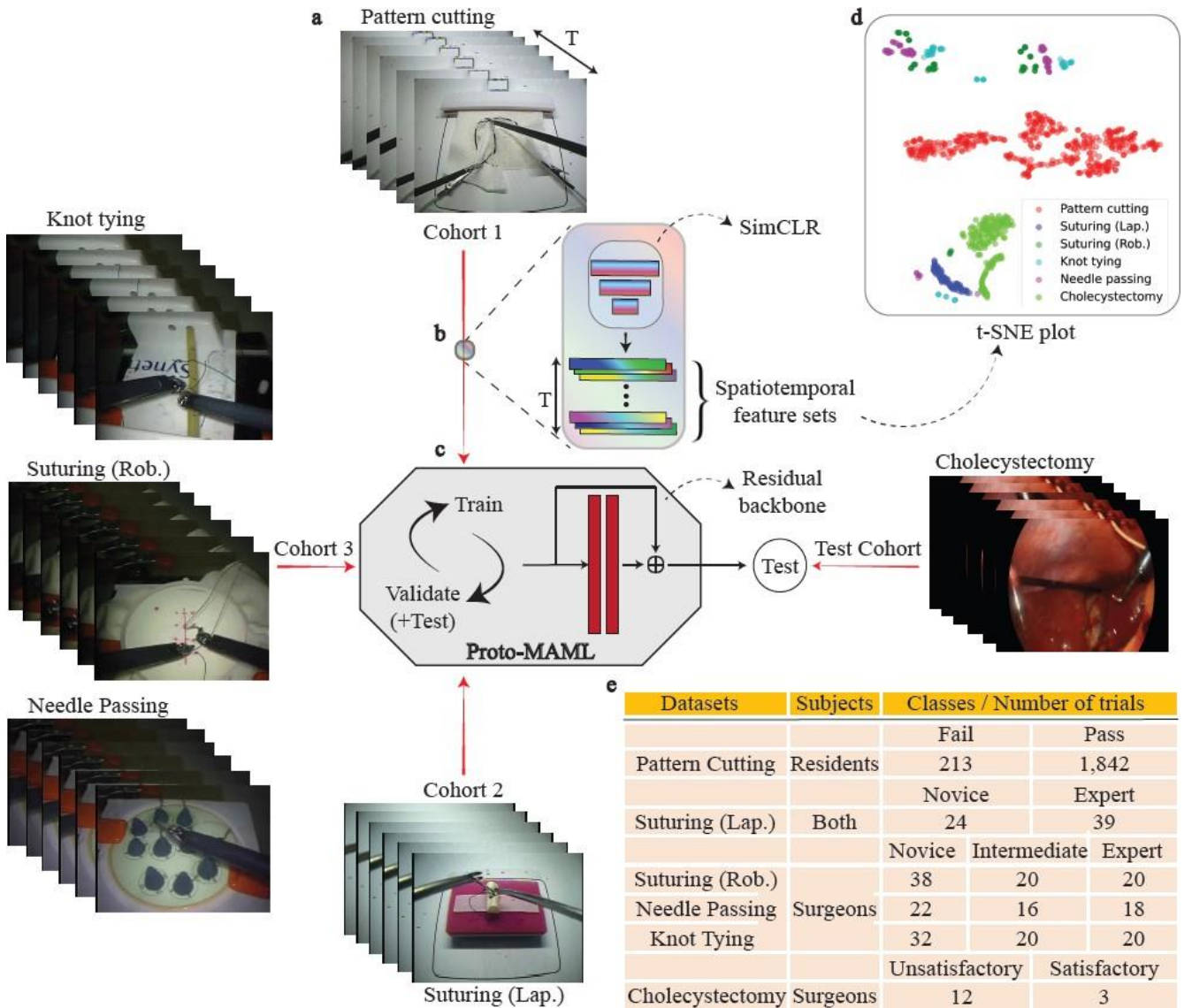


Fig. 1 | A-VBANet Overview. **a.** Metaset comprising various surgical tasks and cohorts. Here, laparoscopic cholecystectomy is an OR surgery, and the remaining are simulators. **b.** Illustration of self-supervised network for spatiotemporal feature extraction (T = temporal length). **c.** Meta-learner pipeline detailing task adaptation, using the residual backbone for sequential inputs. The trained models are tested at each turn in the validation task and laparoscopic cholecystectomy. **d.** t-distributed stochastic neighbor embedding (t-SNE) plot depicting distinct and separable cluster formations of spatiotemporal feature sets across cohorts. **e.** The metaset characteristics.

Pattern cutting involved 21 residents (6 males, 15 females, age 21 - 30; mean 23.95, std. 1.69; 1 left-handed) inexperienced in laparoscopy. Over 12 days, 2,055 trials were conducted, resulting in 1,842 Pass and 213 Fail samples based on the FLS-based cut-off threshold³⁶ (Fig. 1(e)). This produced 1,842 Pass and 213 Fail samples. Videos were collected at 640 x 480 resolution at 30 FPS via the FLS box camera. Suturing, on the other hand, encompassed 10 surgeons (5 males, 5 females) and 8 residents (5

males, 3 females), with ages 23 - 56 (mean: 31, std.: 7.9). All the surgeons had at least one year of experience in FLS, with up to 20 years, while residents had no prior expertise in laparoscopy. This totaled 63 trials (Fig. 1(e)), later classified as 24 Novice (residents) and 39 Expert (surgeons) samples, as using the FLS criterion, we ended up with only three Fail samples. The videos were recorded at 720x480 resolution at 30 FPS via the FLS box camera.

Cohort 3: JIGSAWS tasks. We also employed robotic suturing, needle passing, and knot tying from the publicly available JIGSAWS dataset²¹. For each task, 8 surgeons performed approximately five times on the Da Vinci Surgical System. Surgeons were labeled as Novice (<10 hours of experience), Intermediate, or Expert (> 100 hours of experience). This led to 4 Novice, 2 Intermediate, and 2 Expert surgeons (Fig. 1(e)). In addition, two separate video streams were collected per task from different angles at 640x480 resolution and 30 FPS, treated as separate samples to augment the data size.

Test Cohort: Laparoscopic cholecystectomy. The videos were collected at Kaleida Health in Buffalo, New York, totaling 198 trials. In this study, 15 trials were annotated as Unsatisfactory and Satisfactory, based on the OSATS scores, yielding 12 and 3 samples (Fig. 1(e)), respectively. The criterion for a trial labeled as Satisfactory was having an OSATS score greater than 23 (out of 25) (See Extended Table 5 for the OSATS breakdown). The surgical videos were collected via laparoscopes of varying resolutions at 30 FPS.

Model development. Developing feature extractor. We used Simple Contrastive Learning (SimCLR)³⁷, a self-supervised contrastive network, to automatically extract comprehensive spatiotemporal features without needing manually intensive annotation². Additionally, SimCLR reinforces our pipeline against corrupted frames, e.g., blurry frames and background interference, such as changing light conditions. The model uses a backbone (ResNet34), $f_b(\cdot) \in \mathbb{R}^D$, to aggregate D-(512-)dimensional feature sets, i.e., representations³⁷ from the video frames. Then, using a linear classifier, it maps the representations into K-(128-) dimensional hidden space, $f_h(\cdot) \in \mathbb{R}^K$. The aim is to maximize the likelihood of the classifier finding the augmented versions of the input frame in a large batch of uncorrelated frames in $f_h(\cdot)$ ³⁷. Once trained, the classifier is removed. Extended Fig. 1 illustrates the SimCLR architecture and deployment.

Generating spatiotemporal features. To generate spatiotemporal features (\mathbf{X}), we applied the trained backbone, $f_b(\cdot)$, to each frame in a surgical video in temporal order, i.e., $\mathbf{X}_i = [f_b(x_{i1}), \dots, f_b(x_{ij}), \dots, f_b(x_{iT})] \in \mathbb{R}^{TxD}$, where $x_i \in \mathbb{R}^{Tx3}$ is the list of frames of the i^{th} trial. Here, T is the temporal length and x_{ij} is the i^{th} trial's j^{th} frame. Finally, $\mathbf{X}_i \in \mathbb{R}^{TxD}$ is the spatiotemporal feature set for the i^{th} trial. In addition, we used 1D Global Average Pooling (GAP)³⁸ to downsample D -dimensional representations: $GAP(\mathbf{X}_i) \in \mathbb{R}^{TxD} \rightarrow \mathbf{X}_i' \in \mathbb{R}^{TxD'}$ where D' is of 2,4,8,16,32, and 64.

The meta-learner methodology. ProtoMAML³³ merges the strengths of Prototypical Network (ProtoNet)³² and Model-agnostic Meta-learning (MAML)³⁴. ProtoNet is a metric-based³⁹ meta-learning model, learning to learn prototypical (class) centers, v_c , in nonlinear embedding space³². MAML is a model-based³⁹ meta-learner that offers fast and flexible adaptability to the target domains, learning "global" optimal initialization parameters (θ)³⁴ but lacks robust initialization for the output layer³³. ProtoMAML overcomes this by combining MAML's flexible adaptability with the prototypical center methodology from ProtoNet and reports the best overall performance in multiple image datasets³³. Specifically, ProtoMAML operates by dividing the training and validation sets into support and query sets, where the former optimizes the parameter space, and the latter calculates the train and validation losses. (Supplementary Information / ProtoMAML implementation).

Developing the backbone of the meta-learner. The backbone of the ProtoMAML was derived from our state-of-the-art model, the VBA-Net¹⁷ (Extended Fig. 2). It featured two attention-infused⁴⁰ residual blocks⁴¹ and an intermediate 1x1 convolutional layer³⁸ to adjust the dimension. Each block had two convolutional layers and an identity shortcut¹⁷. Further, the convolutional layers were diluted to expand the receptive field without losing temporal resolution⁴². Notably, dilation proved helpful in improving model performance when working with sequential data¹⁷.

The residual layers were followed by a classifier adjusted to work with the meta-learner. Meta-learning models are used for object classification^{28,32,34}, in which the input is spatial, $x \in \mathbb{R}^{B \times H \times W \times 3}$ (B: batch size, H: height, W: width), and reduced to $\hat{x} \in \mathbb{R}^{B \times D_o}$ by a flattening layer where D_o is the output dimension. However, our input is spatiotemporal, $x \in \mathbb{R}^{B \times T \times D'}$. Hence, the residual blocks were followed by a 1D GAP layer in our design to obtain $\hat{x} \in \mathbb{R}^{B \times D_o}$. GAP also enabled us to use entire sequences. Following GAP, a fully-connected layer generated the embedding space, $f(\hat{x}) \in \mathbb{R}^{D_o}$. Finally, a linear classifier, initialized via v_c , outputted predictions³³. In this study, D_o varied based on D' . (See Supplementary Information / Hyperparameter selection for more information)

Training. Feature extractor. For SimCLR training, we partitioned the datasets via the train/validate split as follows: 143,287/17,373 frames for pattern cutting (cohort 1), 21,191/3,315 for laparoscopic suturing (cohort 2), 447,314/66,836 for the JIGSAWS dataset tasks (cohort 3), and 353,168/46,310 for laparoscopic cholecystectomy (test cohort). Augmentation of input frames followed SimCLR-recommended contrastive transformations³⁷, including horizontal flip, random resized crop, jittering, grayscaling, and Gaussian blur. All the images were normalized prior to training.

We set the minimum number of epochs to 200, employing early stopping with the patience of 10 epochs to terminate training if there is no improvement in accuracy. Large batch sizes in self-supervised learning enhance feature extraction³⁷ by increasing negative samples in the batch, thereby challenging the network to identify augmented pairs more effectively. As a result, we set the mini-batch size to 256 for pattern cutting and 512 for the rest of the tasks.

Meta-learner. Before the training, we downsampled each video stream to 1 FPS. This reduces computational costs¹⁸ while retaining the salient information¹⁷. In addition, training and validation sets underwent separate min-max normalization. We set a minimum of 40 epochs for training, with early stopping with a patience of 10. The mini-batch size was 8.

ProtoMAML necessitates an equal number of samples per class³². The absence of this rule causes an inflated representation of some classes, leading to biased, i.e., domain-specific, estimations. However, in our study, each skill class had a different sample size (Fig. 1(e)). Therefore, we ran each round 100 times with different seeds. We removed the outlier performances based on accuracies using the Tukey Fences⁴³ method. For each repetition, we randomly sampled Ntrain and Nval trials from each class, where Ntrain and Nval are the smallest sample sizes in a class among all the classes in the training and validation sets.

Another limitation is that the model needs the same input size for each mini-batch. However, our data was spatiotemporal with varying lengths, both inter- and intra-tasks. Hence, we incorporated mini-batch zero padding to ProtoMAML. Notably, we did not zero-pad the entire input based on the longest sequence, as that would increase the computational load for shorter tasks significantly.

Evaluation. We used a round-robin scheme to evaluate the A-VBANet, using one task per round for

validation and testing and the remainder for training. For instance, when pattern cutting was the target domain, the remaining tasks were the source domain, i.e., the training domain of the network. Notably, laparoscopic cholecystectomy was excluded from this scheme. Instead, we used the test cohort to further test the trained model’s adaptability in real-life surgery at each round (Fig. 1). We averaged the results from all rounds to obtain the overall adaptation performance. During testing, few-test-shots (k) were used to adapt to the new domain. The rest of the samples were utilized to compute the performance. For multi-class tasks, the accuracies were micro-averaged. Models were developed on Pytorch, and training was conducted via the IBM Artificial Intelligence Multiprocessing Optimized System (AiMOS) at Rensselaer Polytechnic Institute on 8 NVIDIA Tesla V100 GPUs, each with 32 GB capacity.

Results

Here, the results of a task are given for the best spatiotemporal feature set (2-64) via one-test-shot ($k = 1$), an average of 100 repetitions for cohorts 1- 3, and the best of 100 repetitions for the test cohort.

A-VBANet adapts to binary class tasks. In pattern cutting, the adaptation accuracy was 0.900 ± 0.023 (Table 1). We also report the area under curve (AUC) of the Receiver Operating Characteristics (ROC) to be 0.955 ± 0.020 . In laparoscopic suturing, these values were 0.995 ± 0.008 and 0.999 ± 0.005 for accuracy and AUC. Fig. 2(a) illustrates the ROC curves for pattern cutting and suturing. In addition, accuracy increased with k , i.e., few-test-shots, for both tasks (Table 1 and Extended Table 1).

We also evaluated the reliability of the true predictions in each skill class using trust spectrums and the corresponding NetTrustScore (NTS)⁴⁴ (Supplementary Information / NetTrustScore). In pattern cutting, NTSs were 0.989 ± 0.068 for Fail and 0.991 ± 0.047 for Pass. In laparoscopic suturing, NTSs were 0.991 ± 0.009 for Novice and 0.998 ± 0.005 for Expert. NTS increased with k in both tasks (Extended Table 2). Fig. 2(b) details the trust spectrum for the binary class tasks, i.e., cohorts 1 and 2.

Table 1 | Simulation task adaptation accuracies with increasing k values.

Dataset	$k = 1$	$k = 2$	$k = 4$	$k = 8$	$k = 16$
Pattern Cutting	0.900 ± 0.023	0.910 ± 0.022	0.920 ± 0.018	0.925 ± 0.019	0.929 ± 0.017
Suturing (Laparoscopic)	0.995 ± 0.008	0.995 ± 0.008	0.995 ± 0.006	0.997 ± 0.006	0.999 ± 0.005
Suturing (Robotic)	0.651 ± 0.040	0.664 ± 0.027	0.697 ± 0.039	0.716 ± 0.035	0.761 ± 0.044
Needle Passing	0.626 ± 0.027	0.645 ± 0.022	0.690 ± 0.033	0.727 ± 0.038	N/A
Knot Tying	0.688 ± 0.022	0.697 ± 0.031	0.714 ± 0.042	0.763 ± 0.057	0.835 ± 0.077

A-VBANet adapts to multi-class tasks. The adaptation accuracies were 0.651 ± 0.040 , 0.626 ± 0.027 , and 0.688 ± 0.022 in robotic suturing, needle passing, and knot tying (Table 1). The model’s performance increased with k in all tasks (Extended Table 1). Notably, $k = 16$ was not observed in needle passing due to insufficient data. In addition, for true predictions, the NTSs were 0.998 ± 0.003 , 0.994 ± 0.008 , and 0.994 ± 0.008 for Novice, Intermediate, and Expert in robotic suturing. In needle passing, these values were 0.981 ± 0.020 , 0.978 ± 0.022 , and 0.965 ± 0.026 . Finally, in knot tying, we obtained 0.921 ± 0.039 , 0.868 ± 0.052 , and 0.817 ± 0.065 . NTS increased with k in all tasks (Extended Table 2). Fig. 3 illustrates the trust spectrum for the multi-class tasks, i.e., cohort 3.

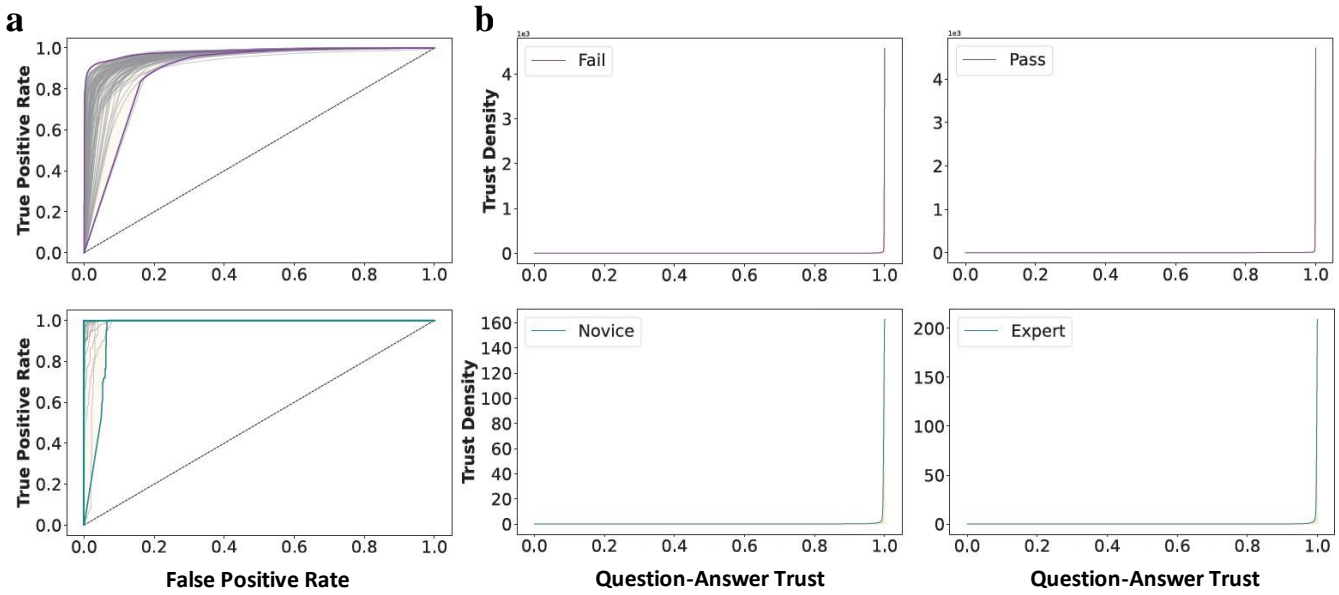


Fig. 2 | a. ROCs. **b.** trust spectrums in pattern cutting (purple) and laparoscopic suturing (turquoise). The y-axis represents the distribution of trustworthiness for each sample, while the x-axis reflects the model's confidence in its predictions.

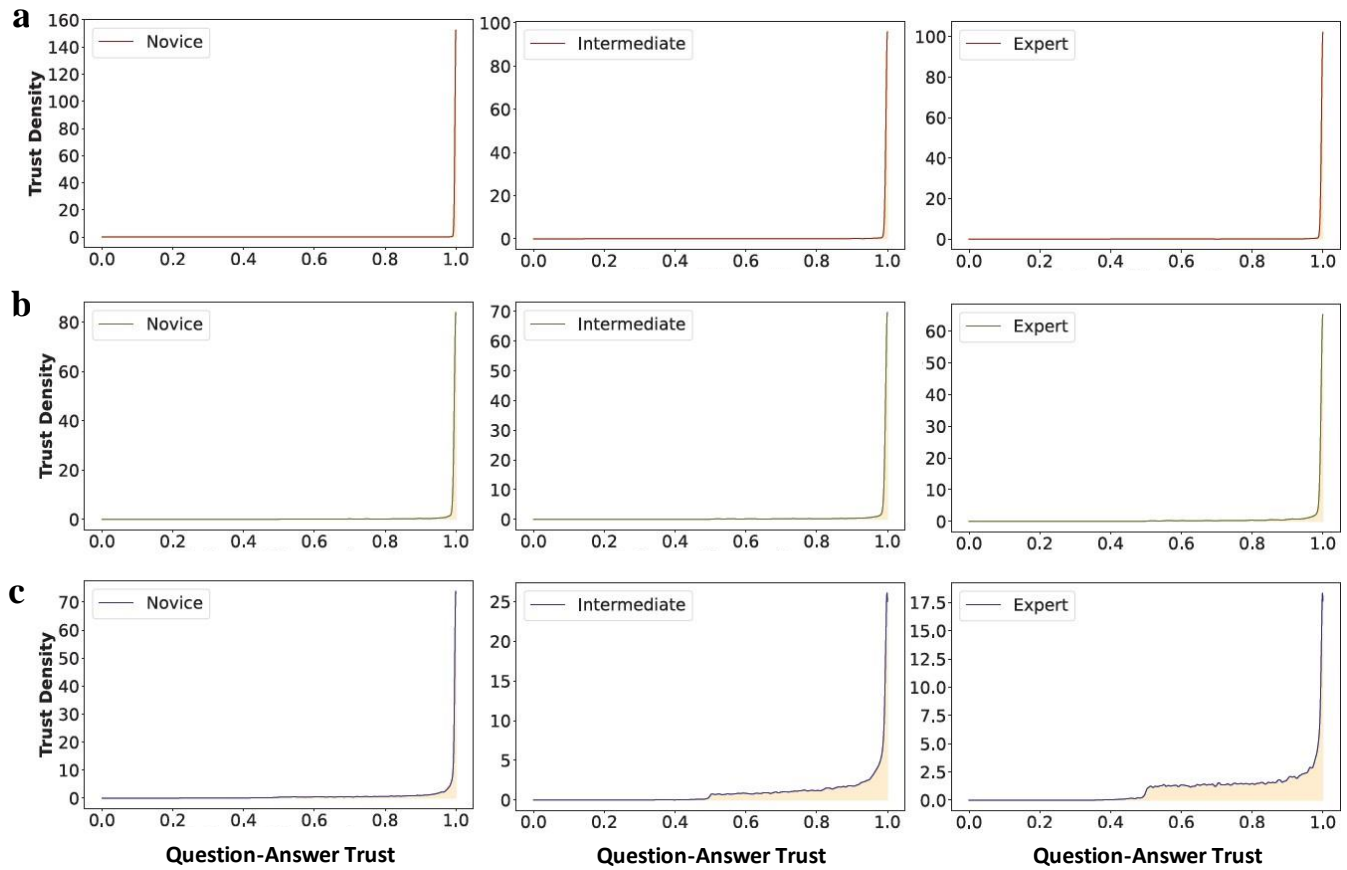


Fig. 3 | Trust spectrums for $k = 1$ cumulative of 100 runs in **a.** robotic suturing, **b.** needle passing, and **c.** knot tying. The y-axis represents the distribution of trustworthiness for each sample, while the x-axis reflects the model's confidence in its predictions.

A-VBANet adapts to an operating room (OR) procedure. After being validated on a different simulator each round, we tested how well the A-VBANet can perform on laparoscopic cholecystectomy. The results are reported in Table 2. We obtained an accuracy of 0.867 and an AUC of 0.840. We did not analyze the few-shot setting due to limited data. When we broke down the performance in individual validation tasks, we observed consistency between the tasks (Table 2 and Extended Table 3). In addition, the NTSs for true predictions were 1.0 for both the Unsatisfactory and Satisfactory classes (Extended Table 4). Fig. 4 shows the trust spectrums for the test cohort.

Table 2 | Adaptation accuracies on the test cohort – laparoscopic cholecystectomy – for $k = 1$.

Validation dataset	Accuracy	AUC
Pattern Cutting	0.872	0.818
Suturing (Laparoscopic)	0.872	0.848
Suturing (Robotic)	0.821	0.833
Needle Passing	0.872	0.838
Knot Tying	0.897	0.864
Overall	0.867	0.840

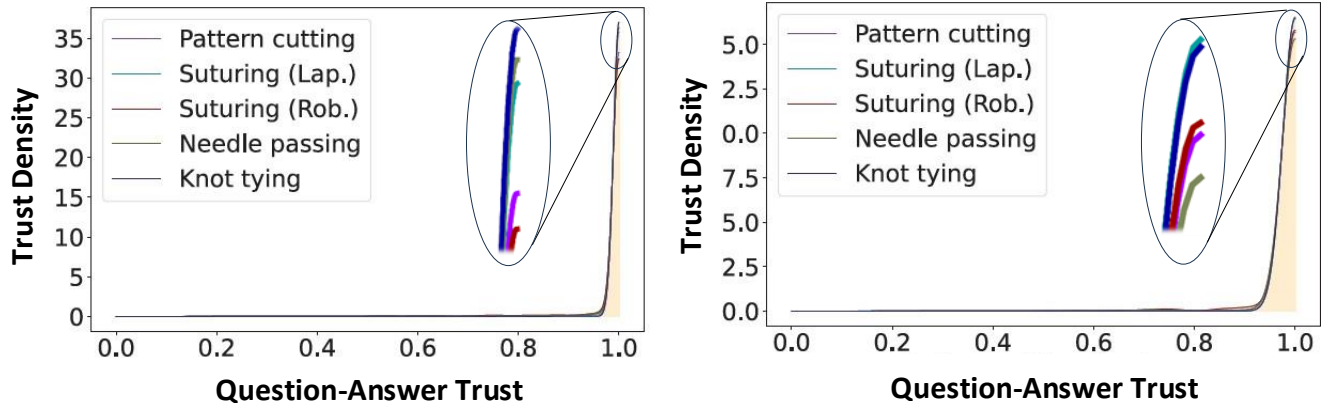


Fig. 4 | Trust spectrums for each validation task for $k = 1$ in laparoscopic cholecystectomy for unsatisfactory (left) and satisfactory (right) classes. The y-axis represents the distribution of trustworthiness for each sample, while the x-axis reflects the model’s confidence in its predictions.

Discussion

In this study, we introduced A-VBANet, a novel meta-learning model for surgical skill assessment, addressing the significant challenges faced by traditional DL approaches. Our development of A-VBANet responds to the crucial need for effective domain adaptation in environments where data is scarce² and specific to particular training domains. By utilizing one-(few-)shot learning, A-VBANet is designed to adapt to a range of surgical tasks, offering a domain-agnostic skill evaluation in both simulated and real-world surgical settings.

Surgical simulators, known for their safety and ability to provide repetitive practice, are integral to surgical training^{2,45-47} and credentialing^{35,48}. Recognizing their importance, we evaluated the adaptability of the A-VBANet in several surgical simulators including two (cohorts 1 and 2) required for board certification in general and obstetrics and gynecology (ob/GYN) surgery³⁵. Our results (Table 1) demonstrated the model's successful adaptation with as few as one sample, significantly influencing training and credentialing processes. For training, our methodology allows expansion into specialized areas with limited data, enhancing trainee skill sets for varied surgical simulator tasks. In credentialing, its adaptability ensures robust competency assessments, crucial for certifying resident proficiency in high-stakes specialties. These implications are not only restricted to surgical domains but also can apply to similar high-stakes disciplines where training and credentialing are essential.

A major challenge in DL for surgical skill assessment is the collection and annotation of data in the OR, an unregulated and resource-intensive environment. This difficulty is compounded by the limited availability of extensive datasets, often restricted by companies and medical societies for proprietary reasons. Such constraints hinder the widespread application of DL in this domain. In response to this challenge, we successfully adapted A-VBANet using surgical simulator data for OR settings, a crucial step for lifelong learning⁴⁹ and continuous certification⁵⁰⁻⁵². Our model demonstrated robust performance in laparoscopic cholecystectomy procedures (Table 2), proving its feasibility in the OR with only one adaptation sample ($k = 1$). Although preliminary, these results are encouraging and suggest that extending A-VBANet to a broader spectrum of procedures and clinical settings could further enhance its performance and utility.

In the field of surgical skill assessment, gauging the trustworthiness of predictive models like A-VBANet is crucial, particularly when making high-stakes decisions. To assess this, we introduced the trust spectrum and NTS⁴⁴. The trust spectrums in Figures 2(b), 3, and 4 show a notable concentration of predictions at higher confidence intervals, indicating that the model consistently makes predictions with high certainty. This high confidence accumulation is quantitatively captured in the robust NTS (Tables 1 and 2). High NTS scores imply that A-VBANet can be trusted to accurately assess surgical skills on unseen data, which is vital for surgical training and credentialing, ensuring that trainees and surgeons are evaluated accurately. Furthermore, it is essential in adapting to OR, where precise skill assessment in complex scenarios is crucial for ensuring surgical competence and patient safety.

We also explored the few-test-shot ($k > 1$) setting for all the tasks, excluding laparoscopic cholecystectomy. The accuracies increased with k (Table 1 | Extended Tables 1), aligning with the expectations since higher k provides more data for the model to adapt to a new domain. However, increasing k reduces the number of available testing samples, leading to heightened epistemic uncertainty⁵³. This can be seen in increasing standard deviation in accuracy values (Table 1) in tasks with limited sample size (Fig. 1) such as the JIGSAWS tasks. On the other hand, while the NTS improved in laparoscopic pattern cutting and suturing, this trend was not consistent across other tasks due to constraint sample size (Extended Tables 2). To draw more definitive conclusions about the NTS, further testing with more extensive datasets is warranted.

The efficacy of self-supervised contrastive learning is gauged in downstream tasks, which, in our study, are represented by A-VBANet's skill assessment results. Despite variations in downsampled spatiotemporal feature sets, our model consistently achieved robust accuracies, underscoring the success of the self-supervised learning approach (Extended Tables 1 and 3). Interestingly, our analysis revealed no direct correlation between the size of these feature sets and the reported accuracies. On the other

hand, increased spatiotemporal feature sizes led to increased NTS values (Extended Tables 2 and 4). This signifies that more information leads to higher confidence in true predictions. However, it decreases the possibility of cross-overs, e.g., false prediction being predicted correctly. This makes the model less flexible and more prone to overfitting.

A key advantage of our study is using videos over sensor-based kinematics, as the latter is more expensive to collect and often unavailable². Videos are not only increasingly more available⁵⁴ but also align with the current shift towards video-based assessment (VBA) by national institutions^{49,55} as a replacement for traditional intraoperative training^{1,22,54}. Besides, this approach enabled us to derive additional information from unlabeled data. For instance, our self-supervision model for the laparoscopic cholecystectomy cohort was trained on 198 videos despite only 15 being labeled. Notably, while our study contended with limited data availability, we consciously chose not to employ the snippetting technique^{5,8,56} to augment the data size. This is because it may inflate the score prediction^{17,22}. Moreover, it causes inconsistent labeling as it is uncertain that performance is isotropic within each trial¹⁷.

Some limitations of our study include cohort-specific preprocessing and limited testing data and tasks. Our future research will focus on integrating meta-learning with self-supervision to address these challenges. This integration aims to facilitate cohort-agnostic feature extraction from video data, paving the way for a more comprehensive end-to-end pipeline for domain adaptation. Additionally, we intend to expand our research to include a wider variety of surgical tasks, enhancing the model's applicability and robustness across different surgical domains.

Conclusion

Our study with A-VBANet marks a significant advancement in surgical skill assessment through the application of DL and meta-learning. We have demonstrated the model's ability to adapt to diverse surgical tasks, from simulator-based exercises to complex OR procedures like laparoscopic cholecystectomy, using as little as one sample. The high accuracies and robust trustworthiness of our model not only enhance its applicability in surgical training and credentialing but also extending its implications to various high-stakes, skill-intensive disciplines with scarce data. Moving forward, we will concentrate on leveraging meta-learning to directly predict performance scores and generate formative feedback further expanding the model's utility in adapted cohorts.

References

1. Hung, A. J. *et al.* Deep learning to automate technical skills assessment in robotic surgery. *BJU Int* **124**, 487–495 (2019).
2. Yanik, E. *et al.* Deep neural networks for the assessment of surgical skills: A systematic review. *Journal of Defense Modeling and Simulation* **19**, 159–171 (2022).
3. Anh, N. X., Nataraja, R. M. & Chauhan, S. Towards near real-time assessment of surgical skills: A comparison of feature extraction techniques. *Comput Methods Programs Biomed* **187**, 105234 (2020).
4. Castro, D., Pereira, D., Zanchettin, C., MacEdo, D. & Bezerra, B. L. D. Towards optimizing convolutional neural networks for robotic surgery skill evaluation. in *Proceedings of the International Joint Conference on Neural Networks (IJCNN)* 1–8 (IEEE, 2019). doi:10.1109/IJCNN.2019.8852341.
5. Doughty, H., Damen, D. & Mayol-Cuevas, W. Who's better? Who's best? Pairwise deep ranking for skill determination. in *IEEE Conference on Computer Vision and Pattern Recognition (CVPR)* 6057–6066 (IEEE, 2018).
6. Fathollahi, M. *et al.* Video-based surgical skills assessment using long term tool tracking. in *International Conference on Medical Image Computing and Computer-Assisted Intervention (MICCAI)* 541–550 (Springer, Cham, 2022).
7. Fawaz, H. I., Forestier, G., Weber, J., Idoumghar, L. & Muller, P.-A. Evaluating surgical skills from kinematic data using convolutional neural networks. in *International Conference on Medical Image Computing and Computer-*

Assisted Intervention (MICCAI) 214–221 (Springer, 2018). doi:10.1007/978-3-030-00937-3.

8. Funke, I., Mees, S. T., Weitz, J. & Speidel, S. Video-based surgical skill assessment using 3D convolutional neural networks. *Int J Comput Assist Radiol Surg* **14**, 1217–1225 (2019).
9. Khalid, S., Goldenberg, M., Grantcharov, T., Taati, B. & Rudzicz, F. Evaluation of Deep Learning Models for Identifying Surgical Actions and Measuring Performance. *JAMA Netw Open* **3**, e201664 (2020).
10. Lajko, G., Elek, R. N. & Haidegger, T. Endoscopic image-based skill assessment in robot-assisted minimally invasive surgery. *Foot Ankle Spec* **14**, 153–157 (2021).
11. Lajkó, G., Elek, R. N. & Haidegger, T. Surgical Skill Assessment Automation Based on Sparse Optical Flow Data. *INES 2021 - IEEE 25th International Conference on Intelligent Engineering Systems, Proceedings* 201–208 (2021) doi:10.1109/INES52918.2021.9512917.
12. Ming, Y. *et al.* Surgical skills assessment from robot assisted surgery video data. in *Proceedings of 2021 IEEE International Conference on Power Electronics, Computer Applications (ICPECA)* 392–396 (IEEE, 2021). doi:10.1109/ICPECA51329.2021.9362525.
13. Nguyen, X. A., Ljuhar, D., Pacilli, M., Nataraja, R. M. & Chauhan, S. Surgical skill levels: Classification and analysis using deep neural network model and motion signals. *Comput Methods Programs Biomed* **177**, 1–8 (2019).
14. Soleymani, A., Li, X. & Tavakoli, M. Deep Neural Skill Assessment and Transfer: Application to Robotic Surgery Training. *IEEE International Conference on Intelligent Robots and Systems* 8822–8829 (2021) doi:10.1109/IROS51168.2021.9636627.
15. Wang, Y. *et al.* Evaluating robotic-assisted surgery training videos with multi-task convolutional neural networks. *J Robot Surg* **16**, 917–925 (2021).
16. Wang, Z. & Fey, A. M. SATR-DL: Improving Surgical Skill Assessment and Task Recognition in Robot-Assisted Surgery with Deep Neural Networks. *Proceedings of the Annual International Conference of the IEEE Engineering in Medicine and Biology Society, EMBS 2018-July*, 1793–1796 (2018).
17. Yanik, E., Kruger, U., Intes, X., Rahul, R. & De, S. Video-based formative and summative assessment of surgical tasks using deep learning. *Sci Rep* **13**, 1–11 (2023).
18. Jin, A. *et al.* Tool detection and operative skill assessment in surgical videos using region-based convolutional neural networks. in *Proceedings - 2018 IEEE Winter Conference on Applications of Computer Vision (WACV)* 691–699 (IEEE, 2018). doi:10.1109/WACV.2018.00081.
19. Srivastav, V. *et al.* MVOR: A multi-view RGB-D operating room dataset for 2D and 3D human pose estimation. <http://arxiv.org/abs/1808.08180> (2018) doi:10.48550/arXiv.1808.08180.
20. Twinanda, A. P. *et al.* EndoNet: A deep architecture for recognition tasks on laparoscopic videos. *IEEE Trans Med Imaging* **36**, 86–97 (2017).
21. Gao, Y. *et al.* JHU-ISI gesture and skill assessment working set (JIGSAWS): A surgical activity dataset for human motion modeling. *Modeling and Monitoring of Computer Assisted Interventions (M2CAI) – MICCAI Workshop* **3**, (2014).
22. Pugh, C. M., Hashimoto, D. A. & Korndorffer, J. R. The what? how? and who? of video based assessment. *Am J Surg* **221**, 13–18 (2021).
23. Zhang, D. *et al.* Automatic Microsurgical Skill Assessment Based on Cross-Domain Transfer Learning. *IEEE Robot Autom Lett* **5**, 4148–4155 (2020).
24. Gevaert, O. Meta-learning reduces the amount of data needed to build AI models in oncology. *Br J Cancer* **125**, 309–310 (2021).
25. Ma, J. *et al.* Few-shot learning creates predictive models of drug response that translate from high-throughput screens to individual patients. *Nat Cancer* **2**, 233–244 (2021).
26. Sun, Q., Liu, Y., Chua, T. & Schiele, B. Meta-transfer learning for few-shot learning. in *Proceedings of the IEEE/CVF Conference on Computer Vision and Pattern Recognition (CVPR)* 403–412 (IEEE, 2019).
27. Walsh, R., Abdelpakey, M. H., Shehata, M. S. & Mohamed, M. M. Automated human cell classification in sparse datasets using few-shot learning. *Sci Rep* **12**, 1–11 (2022).
28. Zhao, Z. *et al.* One to many: Adaptive instrument segmentation via meta learning and dynamic online adaptation in robotic surgical video. in *IEEE International Conference on Robotics and Automation (ICRA)* 13553–13559 (IEEE, 2021). doi:10.1109/ICRA48506.2021.9561690.
29. Stanley, K. O., Clune, J., Lehman, J. & Miikkulainen, R. Designing neural networks through neuroevolution. *Nat Mach Intell* **1**, 24–35 (2019).
30. Zador, A. M. A critique of pure learning and what artificial neural networks can learn from animal brains. *Nat Commun* **10**, 1–7 (2019).
31. Javed, K. & White, M. Meta-learning representations for continual learning. *Adv Neural Inf Process Syst* **32**, 1–11 (2019).
32. Snell, J., Swersky, K. & Zemel, R. Prototypical networks for few-shot learning. in *Advances in Neural Information*

Processing Systems 30 (NeurIPS) 4078–4088 (NeurIPS Proceedings, 2017).

33. Triantafillou, E. *et al.* *Meta-dataset: A dataset of datasets for learning to learn from few examples.* (2020) doi:10.48550/arXiv.1903.03096.

34. Finn, C., Abbeel, P. & Levine, S. Model-agnostic meta-learning for fast adaptation of deep networks. in *34th International Conference on Machine Learning (ICML)* vol. 3 1856–1868 (PMLR, 2017).

35. Fried, G. M. FLS assessment of competency using simulated laparoscopic tasks. *Journal of Gastrointestinal Surgery* **12**, 210–212 (2008).

36. Fraser, S. A. *et al.* Evaluating laparoscopic skills, setting the pass/fail score for the MISTELS system. *Surgical Endoscopy and Other Interventional Techniques* **17**, 964–967 (2003).

37. Chen, T., Kornblith, S., Norouzi, M. & Hinton, G. E. A simple framework for contrastive learning of visual representations. in *Proceedings of the 37th International Conference on Machine Learning (ICML)* 1597–1607 (PMLR, 2020).

38. Lin, M., Chen, Q. & Yan, S. *Network in network.* (2014) doi:10.48550/arXiv.1312.4400.

39. Tian, Y., Zhao, X. & Huang, W. Meta-learning approaches for learning-to-learn in deep learning: A survey. *Neurocomputing* **494**, 203–223 (2022).

40. Hu, J., Shen, L. & Sun, G. Squeeze-and-excitation networks. in *Proceedings of the IEEE Computer Society Conference on Computer Vision and Pattern Recognition (CVPR)* 7132–7141 (IEEE, 2018).

41. He, K., Zhang, X., Ren, S. & Sun, J. Deep Residual Learning for Image Recognition. in *Proceedings of the IEEE Computer Society Conference on Computer Vision and Pattern Recognition (CVPR)* 770–778 (IEEE, 2006). doi:10.1109/cvpr.2006.50130.

42. Yu, F. & Koltun, V. Multi-scale context aggregation by dilated convolutions. *4th International Conference on Learning Representations, ICLR 2016 - Conference Track Proceedings* (2016).

43. Hoaglin, D. C. Tukey and data analysis. *Statistical Science* **18**, 311–318 (2003).

44. Wong, A., Wang, X. Y. & Hryniowski, A. *How much can we really trust you? Towards simple, interpretable trust quantification metrics for deep neural networks.* arXiv (2020) doi:10.48550/arXiv.2009.05835.

45. Brinkman, W. M. *et al.* Da vinci skills simulator for assessing learning curve and criterion-based training of robotic basic skills. *Urology* **81**, 562–566 (2013).

46. Korndorffer, J. R. *et al.* Simulator training for laparoscopic suturing using performance goals translates to the operating room. *J Am Coll Surg* **201**, 23–29 (2005).

47. Sroka, G. *et al.* Fundamentals of laparoscopic surgery simulator training to proficiency improves laparoscopic performance in the operating room-a randomized controlled trial. *Am J Surg* **199**, 115–120 (2010).

48. Hafford, M. L. *et al.* Ensuring competency: Are fundamentals of laparoscopic surgery training and certification necessary for practicing surgeons and operating room personnel? *Surg Endosc* **27**, 118–126 (2013).

49. Feldman, L. S. *et al.* SAGES Video-based assessment (VBA) program: a vision for life-long learning for surgeons. *Surg Endosc* **34**, 3285–3288 (2020).

50. Pradarelli, J. C. *et al.* Surgical coaching to achieve the ABMS vision for the future of continuing board certification. *Am J Surg* **221**, 4–10 (2021).

51. Esposito, A. C., Coppersmith, N. A., White, E. M. & Yoo, P. S. Video coaching in surgical education: Utility, opportunities, and barriers to implementation. *J Surg Educ* **79**, 717–724 (2021).

52. Statement on continuous certification. <https://www.sages.org/publications/guidelines/statement-on-continuous-certification/>.

53. Abdar, M. *et al.* A review of uncertainty quantification in deep learning: Techniques, applications and challenges. *Information Fusion* **76**, 243–297 (2021).

54. McQueen, S., McKinnon, V., VanderBeek, L., McCarthy, C. & Sonnadara, R. Video-Based assessment in surgical education: a scoping review. *J Surg Educ* **76**, 1645–1654 (2019).

55. ABS to explore video-based assessment in pilot program launching june 2021. https://www.absurgery.org/default.jsp?news_vba04.21.

56. Fathabadi, F. R., Grantner, J. L., Shebrain, S. A. & Abdel-Qader, I. Surgical Skill Assessment System Using Fuzzy Logic in a Multi-Class Detection of Laparoscopic Box-Trainer Instruments. *Conf Proc IEEE Int Conf Syst Man Cybern* 1248–1253 (2021) doi:10.1109/SMC52423.2021.9658766.

Data availability

Our group collected the laparoscopic pattern cutting and suturing datasets under IRB regulations, and the deidentified source frames and class labels will be released upon publication.

Acknowledgments

The authors graciously acknowledge Dr. Yuanyuan Gao for assisting with the pattern cutting video data collection and Dr. Lora Cavuoto for spearheading the laparoscopic suturing experiments and data collection.

Author contributions

E.Y. and S.D. conceived the idea. E.Y. designed the analysis, developed the network, trained the pipeline, and drafted the manuscript. S.D. and X.I. were responsible for supervising and revising the manuscript. J.N. and M.H. helped with goal setting and provided feedback throughout the study. S.S. and G.Y. collected the laparoscopic cholecystectomy videos, and G.Y. provided corresponding OSATS scores.

Competing Interests

The authors declare no competing interests.

Supplementary Information

NetTrustScore (NTS). NTS is a trustworthiness estimation based on the Softmax of predictions¹. NTS builds around the following steps:

Question-answer trust, $Q_z(x, y)$. It quantifies the reliability of the predicted label (y) for a given sample (x) via model M . As seen in Eqn. 1, for true predictions ($R_{y=z}$, z being the actual label / class), the Softmax values, $C(y|x)$, are aggregated via a reward coefficient (α). For the false predictions ($R_{y \neq z}$), the Softmax values were subtracted from 1 with a penalty coefficient (β). In this study, both α and β are 1.

$$Q_z(x, y) = \begin{cases} C(y|x)^\alpha & \text{if } x \in R_{y=z} | M \\ (1 - C(y|x))^\beta & \text{if } x \in R_{y \neq z} | M \end{cases} \quad (1)$$

For conditional trustworthiness², i.e., reliability of a condition such as true predictions or false predictions, we use Eqn. 2 differently than in the original paper (Eqn. 1), as the false predictions are handled separately from the true ones without the need to penalize. In Eqn. 2, R_c is the condition space.

$$Q_c(x, y) = C(y|x)^\alpha \text{ if } x \in R_c | M \quad (2)$$

Trust Density, $F(Q_c)$. It is the trust behavior of the model for all the samples (xs) in a given condition. It is obtained via non-parametric density estimation through Gaussian kernel¹. Here, the bandwidth of the kernel is $\frac{\gamma}{\sqrt{N}}$ with $\gamma = 0.5$ and $N = \text{length}(x)$.

Trust Spectrum, $T_M(c)$. It is the trust behavior of the network for all the conditions in a dataset, as given in Eqn. 3. In the equation, $T_M(c)$, outputs a list of overall trustworthiness for each condition.

$$T_M(c) = \frac{1}{N} \int Q_c(x) dx \quad (3)$$

NetTrustScore, NTS. Based on the original proposal, NTS is the overall trustworthiness score of the network via all the predictions and classes and scales from 0 to 1. However, in this study, when we report NTS, it is not global but for a condition instead as governed by Eqns. 2 and 3.

ProtoMAML implementation. ProtoMAML³ is a meta-learner that combines Model-agnostic meta-learning (MAML)⁴ and Prototypical Networks (ProtoNet)⁵.

MAML. In MAML, the model (f) learns the best parameter space (θ) to provide fast and flexible adaptability. In detail, first, θ is randomly initialized, and the input is passed forward(f_θ) for task T_i . Then based on the computed loss (L_{T_i}) in the embedded space, backpropagation is applied to update weights (∇_θ) as shown in Eqn. 4.

$$\theta'_i = \theta - \alpha \nabla_\theta L_{T_i}(f_\theta) \quad (4)$$

Ideally, $f(\theta')$ represents the T_i robustly after several updates, i.e., N_w : the number of updates, same as conventional training. However, in meta-learning, the objective is not to find the optimal parameters for a task but to find the parameters that ensure adaptation. Therefore, we apply Eqn. 4 to each task in the task distribution, $P(T)$, and obtain respective parameter spaces (θ'), which are then passed forward, $f_{\theta'}$, to compute the new loss as seen in Eqn. 5. This way, we obtain the optimal parameter space that minimizes the joint cost function. This step is called the *inner loop*. Thus, in Eqn. 4, α is the *inner learning rate*.

$$\theta = \operatorname{argmin}_\theta \sum_{T_i \sim P(T)} L_{T_i}(f_{\theta'_i}) \quad (5)$$

Next, we update θ based on the optimal parameters from the inner loop, as illustrated in Eqn. 6. This step is called the *outer loop*, and β is the *outer learning rate*.

$$\theta = \theta - \beta \nabla_\theta \sum_{T_i \sim P(T)} L_{T_i}(f_{\theta'_i}) \quad (6)$$

As seen in Eqn. 6, a gradient's gradient is computed, i.e., Hessian-vector product⁴, which is computationally expensive. Thus, the authors of the MAML article⁴ proposed first-order MAML (f-MAML), which only uses the first-order gradients. We also followed this paradigm, hence updated Eqn. 6 as follows:

$$\theta = \theta - \beta \sum_{T_i \sim P(T)} \nabla_{\theta'_i} L_{T_i}(f_{\theta'_i}) \quad (7)$$

ProtoNet. The way the ProtoNet works is detailed as follows. First, the training set is split into support set, $S = [(x_1, y_1), \dots, (x_s, y_s), \dots, (x_N, y_N)]$ and query set, $Q = [(x_1, y_1), \dots, (x_q, y_q), \dots, (x_N, y_N)]$ with N samples. Here, $x_s, x_q \in \mathbb{R}^D$ are inputs whereas y_s and y_q are the corresponding labels in the support and query sets. Then, the model, f_θ , embeds the inputs into M -dimensional feature set, $f_\theta(\cdot) : \mathbb{R}^D \rightarrow \mathbb{R}^M$. Next, using the embedded support set samples, the prototypical center (v_c) is computed as given in Eqn. 8. In the equation, S_c is all the (x_s, y_s) pairs in the support set with $y = c$. Here $c \in \mathcal{C} \mid \mathcal{C}$: all the classes represented in S .

$$v_c = \frac{1}{|S_c|} \sum_{(x_{s,i}, y_{s,i}) \in S_c} f_\theta(x_{s,i}) \quad (8)$$

The query set is then used to compute the loss function (L) based on the distance between the query samples, x_q , and v_c via the distance function, d_φ : the Euclidean Distance.

ProtoMAML. It follows the MAML, specifically fo-MAML, methodology to adapt³, while for the final layer, i.e., the layer that outputs for a specific task, the weights (W_c) and bias (b_c) are initialized based on the v_c as computed in Eqn. 8, instead of random initialization as used by the vanilla fo-MAML. Particularly, the initialization occurs as follows: $W_c = 2v_c$ and $b_c = -||v_c||^2$. For more information, please refer to the original paper³.

Hyperparameter selection. The SimCLR network uses the pretrained ResNet34⁶ - on ImageNet⁷ – as its backbone. Moreover, the pipeline aims to minimize the loss function, InfoNCE (NT-Xent)⁸, via the Adam optimizer with a learning rate of 0.0005. Further, the non-linearity is added via ReLU.

The ProtoMAML minimizes Cosine Similarity Loss⁹ based on Euclidean distance⁵. The inner and outer loop optimizers are Stochastic Gradient Descent (SGD) and Adam, respectively, while the learning rates are 0.1 and 0.01. Moreover, we used a learning rate scheduler in which the rate was factored by 0.6 for every 10 epochs without improving the validation accuracy. Further, N_w , i.e., number of inner loop weight updates, is 1 in training and 20 in testing. Finally, for self-supervised feature (SSF) sets from 2 to 32, the v_c is a 512-dimensional feature vector; for the SSF set of 64, this value is 1,024.

In addition, the meta-learner utilizes an in-house Residual Neural Network (RNN) as the backbone. The filter size is 5 for the convolutional layers of the first residual block. This value is 3 for the second. On the other hand, the dilation rates are 1 and 2, and the stride is 1. Finally, the non-linearity is added using ReLU.

Supplementary Tables

Extended Table 1 | Accuracies for task adaptation. k: number of test shots. Bold values are reported in the manuscript. For needle passing, k = 16 was not investigated as it leaves no Intermediate class for the query set.

Validation and Testing Dataset	SSF set	No. of test-shots				
		k = 1	k = 2	k = 4	k = 8	k = 16
Pattern Cutting	2	0.858±.045	0.871±.044	0.881±.039	0.888±.039	0.892±.037
	4	0.889±.037	0.903±.033	0.910±.032	0.916±.030	0.918±.029
	8	0.900±.023	0.910±.022	0.920±.018	0.925±.019	0.929±.017
	16	0.899±.035	0.910±.034	0.914±.033	0.915±.033	0.914±.035
	32	0.868±.042	0.888±.043	0.896±.039	0.898±.038	0.900±.038
	64	0.821±.066	0.839±.062	0.847±.055	0.853±.048	0.853±.049
Suturing (Lap.)	2	0.987±.012	0.989±.011	0.989±.011	0.990±.011	0.997±.009
	4	0.991±.013	0.988±.019	0.993±.009	0.994±.008	0.999±.005
	8	0.995±.008	0.995±.008	0.995±.006	0.997±.006	0.998±.008
	16	0.990±.013	0.992±.011	0.993±.010	0.992±.011	0.999±.006
	32	0.992±.011	0.992±.012	0.992±.011	0.992±.011	0.999±.005
	64	0.966±.036	0.969±.033	0.971±.032	0.974±.029	0.964±.042
Suturing (Robotic)	2	0.618±.014	0.649±.018	0.649±.029	0.631±.036	0.708±.058
	4	0.625±.014	0.657±.021	0.669±.029	0.686±.041	0.692±.063
	8	0.650±.015	0.659±.018	0.661±.018	0.675±.024	0.662±.035
	16	0.650±.023	0.664±.027	0.697±.039	0.716±.035	0.761±.044
	32	0.644±.022	0.653±.021	0.663±.026	0.686±.038	0.691±.050
	64	0.651±.040	0.679±.050	0.692±.052	0.688±.068	0.740±.091
Needle Passing	2	0.607±.021	0.626±.025	0.666±.033	0.694±.042	
	4	0.616±.018	0.645±.022	0.690±.033	0.727±.038	
	8	0.621±.026	0.637±.029	0.645±.042	0.697±.046	
	16	0.626±.027	0.640±.034	0.666±.040	0.692±.042	N/A
	32	0.614±.027	0.632±.046	0.639±.045	0.683±.054	
	64	0.581±.019	0.587±.026	0.611±.038	0.618±.049	
Knot Tying	2	0.676±.023	0.691±.023	0.698±.032	0.707±.044	0.707±.042
	4	0.688±.022	0.694±.020	0.698±.024	0.742±.036	0.766±.062
	8	0.670±.015	0.686±.021	0.713±.025	0.730±.034	0.786±.057
	16	0.688±.028	0.697±.031	0.714±.042	0.749±.060	0.831±.064
	32	0.673±.026	0.694±.029	0.708±.042	0.763±.057	0.835±.077
	64	0.653±.033	0.673±.043	0.692±.050	0.715±.060	0.733±.078

Extended Table 2 | NTS for true predictions in task adaptation. k: number of test shots. Bold values are reported in the manuscript, selected based on best accuracies in Extended Table 1. For needle passing, k = 16 was not investigated as it leaves no Intermediate class for the query set.

Val. and Testing Dataset	SSF set	Classes	No. of test-shots				
			k = 1	k = 2	k = 4	k = 8	k = 16
Pattern Cutting	2	Fail	0.984±.011	0.984±.012	0.985±.012	0.986±.012	0.986±.013
		Pass	0.988±.009	0.989±.009	0.991±.008	0.991±.008	0.991±.008
	4	Fail	0.986±.007	0.988±.007	0.988±.007	0.989±.007	0.989±.007
		Pass	0.989±.005	0.991±.005	0.992±.005	0.992±.004	0.992±.004
	8	Fail	0.989±.007	0.990±.007	0.990±.007	0.991±.006	0.991±.006
		Pass	0.991±.005	0.993±.004	0.994±.003	0.994±.003	0.994±.003
	16	Fail	0.998±.003	0.999±.002	0.999±.003	0.999±.002	0.999±.003
		Pass	0.999±.002	0.999±.001	0.999±.001	0.999±.001	0.999±.002
	32	Fail	0.997±.004	0.998±.004	0.998±.004	0.998±.005	0.998±.005
		Pass	0.998±.004	0.998±.003	0.999±.003	0.999±.003	0.999±.003
Suturing (Lap.)	64	Fail	1.0	1.0	1.0	1.0	1.0
		Pass	1.0	1.0	1.0	1.0	1.0
	2	Novice	0.968±.027	0.971±.028	0.971±.029	0.973±.027	0.979±.029
		Expert	0.967±.043	0.968±.046	0.966±.049	0.966±.049	0.972±.044
	4	Novice	0.981±.017	0.983±.015	0.984±.014	0.986±.014	0.997±.007
		Expert	0.989±.020	0.988±.024	0.988±.024	0.990±.022	0.990±.025
	8	Novice	0.991±.009	0.992±.010	0.993±.009	0.993±.008	0.987±.018
		Expert	0.998±.005	0.997±.007	0.996±.010	0.996±.009	0.998±.008
	16	Novice	0.997±.005	0.997±.005	0.997±.006	0.997±.006	1.0
		Expert	0.999±.004	0.999±.003	0.999±.002	0.999±.002	0.999±.003
	32	Novice	0.998±.003	0.999±.003	0.998±.003	0.998±.004	0.999±.006
		Expert	1.0	1.0	1.0	1.0	1.0
	64	Novice	1.0	1.0	1.0	1.0	1.0
		Expert	1.0	1.0	1.0	1.0	1.0
Suturing (Robotic)	2	Novice	0.884±.041	0.861±.046	0.888±.054	0.897±.058	0.910±.064
		Interm.	0.818±.057	0.774±.066	0.724±.075	0.759±.096	0.562±.056
		Expert	0.782±.063	0.693±.073	0.661±.071	0.721±.086	0.585±.070
	4	Novice	0.878±.042	0.868±.049	0.886±.054	0.891±.059	0.894±.065
		Interm.	0.820±.058	0.753±.072	0.691±.084	0.637±.098	0.623±.110
		Expert	0.794±.059	0.759±.067	0.692±.073	0.666±.085	0.592±.098
	8	Novice	0.897±.041	0.918±.043	0.929±.042	0.927±.043	0.938±.051
		Interm.	0.757±.062	0.725±.076	0.681±.078	0.582±.060	0.598±.100
		Expert	0.806±.058	0.768±.065	0.681±.073	0.607±.059	0.577±.058
	16	Novice	0.984±.022	0.986±.023	0.989±.028	0.989±.028	0.990±.030

Needle Passing	Knot Tying	32	Novice	0.977 \pm 0.030	0.979 \pm 0.029	0.984 \pm 0.025	0.984 \pm 0.027	0.985 \pm 0.031	
		32	Interm.	0.950 \pm 0.045	0.933 \pm 0.067	0.919 \pm 0.087	0.850 \pm 0.130	0.862 \pm 0.170	
		32	Expert	0.947 \pm 0.048	0.925 \pm 0.067	0.908 \pm 0.092	0.817 \pm 0.140	0.761 \pm 0.210	
		64	Novice	0.998\pm0.003	0.999 \pm 0.003	0.999 \pm 0.003	0.999 \pm 0.002	0.999 \pm 0.006	
		64	Interm.	0.994\pm0.008	0.992 \pm 0.017	0.989 \pm 0.023	0.992 \pm 0.020	0.963 \pm 0.089	
		64	Expert	0.994\pm0.008	0.992 \pm 0.013	0.992 \pm 0.017	0.989 \pm 0.024	0.965 \pm 0.083	
		2	Novice	0.907 \pm 0.041	0.881 \pm 0.061	0.869 \pm 0.080	0.871 \pm 0.110		
		2	Interm.	0.927 \pm 0.038	0.889 \pm 0.054	0.894 \pm 0.068	0.871 \pm 0.110		
		2	Expert	0.878 \pm 0.050	0.804 \pm 0.071	0.760 \pm 0.095	0.698 \pm 0.110		
		4	Novice	0.925 \pm 0.037	0.910 \pm 0.048	0.894 \pm 0.078	0.903 \pm 0.095		
		4	Interm.	0.935 \pm 0.040	0.912 \pm 0.054	0.893 \pm 0.064	0.903 \pm 0.095		
		4	Expert	0.885 \pm 0.050	0.857 \pm 0.066	0.777 \pm 0.095	0.764 \pm 0.120		
		8	Novice	0.939 \pm 0.035	0.920 \pm 0.044	0.905 \pm 0.057	0.894 \pm 0.083		
		8	Interm.	0.953 \pm 0.028	0.909 \pm 0.048	0.906 \pm 0.065	0.946 \pm 0.068		
		8	Expert	0.896 \pm 0.049	0.847 \pm 0.067	0.811 \pm 0.089	0.796 \pm 0.120		
		16	Novice	0.981\pm0.020	0.981 \pm 0.023	0.979 \pm 0.026	0.984 \pm 0.027		N/A
		16	Interm.	0.978\pm0.022	0.974 \pm 0.031	0.969 \pm 0.035	0.984 \pm 0.031		
		16	Expert	0.965\pm0.026	0.955 \pm 0.042	0.947 \pm 0.056	0.946 \pm 0.070		
		32	Novice	0.981 \pm 0.018	0.970 \pm 0.034	0.972 \pm 0.034	0.977 \pm 0.042		
		32	Interm.	0.985 \pm 0.017	0.984 \pm 0.021	0.983 \pm 0.028	0.969 \pm 0.051		
		32	Expert	0.970 \pm 0.028	0.954 \pm 0.044	0.946 \pm 0.056	0.936 \pm 0.075		
		64	Novice	0.996 \pm 0.067	0.998 \pm 0.005	0.997 \pm 0.009	0.997 \pm 0.010		
		64	Interm.	0.997 \pm 0.006	0.996 \pm 0.006	0.993 \pm 0.021	0.993 \pm 0.025		
		64	Expert	0.994 \pm 0.009	0.995 \pm 0.008	0.993 \pm 0.015	0.993 \pm 0.015		
		2	Novice	0.875 \pm 0.053	0.871 \pm 0.055	0.859 \pm 0.068	0.894 \pm 0.070	0.883 \pm 0.080	
		2	Interm.	0.817 \pm 0.064	0.789 \pm 0.075	0.728 \pm 0.091	0.720 \pm 0.100	0.691 \pm 0.120	
		2	Expert	0.776 \pm 0.072	0.743 \pm 0.085	0.699 \pm 0.096	0.639 \pm 0.097	0.629 \pm 0.100	
		4	Novice	0.921\pm0.039	0.924 \pm 0.040	0.907 \pm 0.041	0.935 \pm 0.047	0.934 \pm 0.059	
		4	Interm.	0.868\pm0.052	0.844 \pm 0.061	0.814 \pm 0.079	0.687 \pm 0.120	0.666 \pm 0.140	
		4	Expert	0.817\pm0.065	0.806 \pm 0.063	0.796 \pm 0.071	0.682 \pm 0.120	0.692 \pm 0.120	
		8	Novice	0.926 \pm 0.038	0.923 \pm 0.045	0.923 \pm 0.043	0.928 \pm 0.058	0.949 \pm 0.044	
		8	Interm.	0.875 \pm 0.064	0.831 \pm 0.080	0.791 \pm 0.095	0.740 \pm 0.130	0.736 \pm 0.110	
		8	Expert	0.808 \pm 0.073	0.787 \pm 0.079	0.774 \pm 0.082	0.749 \pm 0.086	0.658 \pm 0.130	
		16	Novice	0.970 \pm 0.029	0.965 \pm 0.034	0.966 \pm 0.036	0.970 \pm 0.041	0.977 \pm 0.039	
		16	Interm.	0.960 \pm 0.049	0.951 \pm 0.057	0.943 \pm 0.075	0.863 \pm 0.140	0.984 \pm 0.130	
		16	Expert	0.919 \pm 0.068	0.928 \pm 0.067	0.923 \pm 0.075	0.892 \pm 0.120	0.866 \pm 0.160	
		32	Novice	0.980 \pm 0.020	0.982 \pm 0.022	0.975 \pm 0.030	0.982 \pm 0.030	0.985 \pm 0.034	
		32	Interm.	0.962 \pm 0.034	0.955 \pm 0.044	0.956 \pm 0.049	0.891 \pm 0.120	0.933 \pm 0.110	
		32	Expert	0.930 \pm 0.056	0.932 \pm 0.058	0.937 \pm 0.060	0.901 \pm 0.120	0.894 \pm 0.140	

	Novice	0.995±.008	0.997±.006	0.997±.007	0.996±.013	0.997±.010
64	Interm.	0.992±.011	0.991±.016	0.991±.020	0.976±.062	0.981±.064
	Expert	0.989±.014	0.990±.016	0.989±.020	0.974±.059	0.972±.080

Extended Table 3 | Accuracies and AUC in cholecystectomy. k: number of test shots. Bold values are reported in the manuscript.

Validation Dataset	SSF set	No. of test-shots		
		k = 1		
		Accuracy	AUC	
Pattern Cutting	2	0.692	0.798	
	4	0.718	0.803	
	8	0.795	0.848	
	16	0.821	0.803	
	32	0.795	0.788	
	64	0.872	0.818	
Suturing (Lap.)	2	0.667	0.747	
	4	0.718	0.841	
	8	0.821	0.864	
	16	0.872	0.848	
	32	0.846	0.848	
	64	0.821	0.818	
Suturing (Robotic)	2	0.718	0.788	
	4	0.718	0.788	
	8	0.769	0.848	
	16	0.615	0.652	
	32	0.795	0.833	
	64	0.821	0.833	
Needle Passing	2	0.872	0.838	
	4	0.846	0.859	
	8	0.846	0.876	
	16	0.692	0.677	
	32	0.692	0.758	
	64	0.872	0.818	
Knot Tying	2	0.667	0.755	
	4	0.564	0.621	
	8	0.795	0.838	
	16	0.872	0.864	
	32	0.615	0.715	

Extended Table 4 | NTS for true predictions in cholecystectomy. k: number of test shots. Bold values are used to obtain average NTSs, as reported in the manuscript. They are selected based on the best accuracies in Extended Table 3.

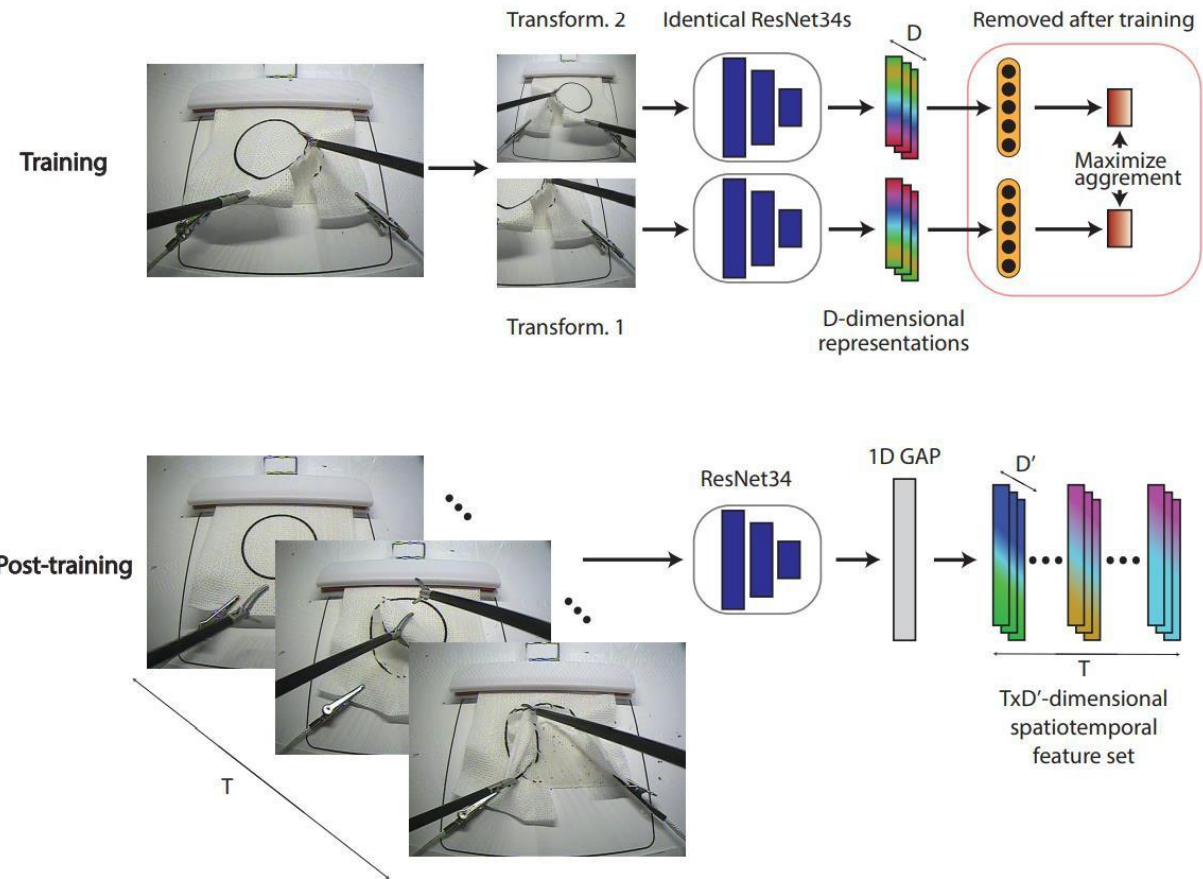
Validation Dataset	SSF set	Classes	No. of test-shots	
			k = 1	
Pattern Cutting	2	Unsatisfactory	1.0	
		Satisfactory	1.0	
	4	Unsatisfactory	1.0	
		Satisfactory	1.0	
	8	Unsatisfactory	1.0	
		Satisfactory	1.0	
	16	Unsatisfactory	1.0	
		Satisfactory	1.0	
	32	Unsatisfactory	1.0	
		Satisfactory	1.0	
Suturing (Lap.)	64	Unsatisfactory	1.0	
		Satisfactory	1.0	
	2	Unsatisfactory	1.0	
		Satisfactory	1.0	
	4	Unsatisfactory	1.0	
		Satisfactory	1.0	
	8	Unsatisfactory	1.0	
		Satisfactory	1.0	
	16	Unsatisfactory	1.0	
		Satisfactory	1.0	
Suturing (Robotic)	32	Unsatisfactory	1.0	
		Satisfactory	1.0	
	64	Unsatisfactory	1.0	
		Satisfactory	1.0	
	2	Unsatisfactory	1.0	
		Satisfactory	1.0	
	4	Unsatisfactory	1.0	
		Satisfactory	1.0	
	8	Unsatisfactory	1.0	
		Satisfactory	1.0	
	16	Unsatisfactory	1.0	
		Satisfactory	1.0	
	32	Unsatisfactory	1.0	
		Satisfactory	1.0	

Needle Passing	64	Unsatisfactory	1.0
		Satisfactory	1.0
	2	Unsatisfactory	1.0
		Satisfactory	1.0
	4	Unsatisfactory	1.0
		Satisfactory	1.0
	8	Unsatisfactory	1.0
		Satisfactory	1.0
	16	Unsatisfactory	1.0
		Satisfactory	1.0
Knot Tying	32	Unsatisfactory	1.0
		Satisfactory	1.0
	64	Unsatisfactory	1.0
		Satisfactory	N/A
	2	Unsatisfactory	1.0
		Satisfactory	1.0
	4	Unsatisfactory	1.0
		Satisfactory	1.0
	8	Unsatisfactory	1.0
		Satisfactory	1.0
Mean	16	Unsatisfactory	1.0
		Satisfactory	1.0
	32	Unsatisfactory	1.0
		Satisfactory	1.0
	64	Unsatisfactory	1.0
		Satisfactory	1.0
Mean	Unsatisfactory	1.0	
	Satisfactory	1.0	

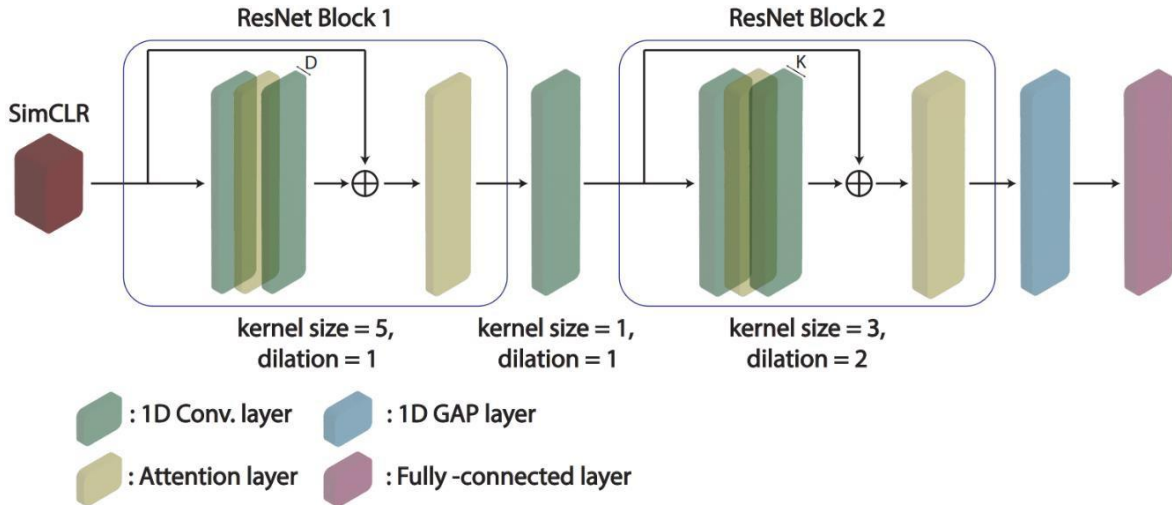
Extended Table 5 | OSATS scores breakdown.

OSATS score	Number of trials	Assigned label
13	1	Unsatisfactory
15	1	
16	2	
18	1	
19	1	
20	1	
21	2	
22	1	
23	2	
24	2	Satisfactory

Supplementary Figures



Extended Fig. 1 | SimCLR architecture and spatiotemporal feature set generation. D represents the output dimension of the SimCLR once trained while D' is the dimension after the 1D GAP layer. T is the temporal length of a given sample. Pattern cutting frames were used to represent the pipeline.



Extended Fig. 2 | The backbone of the pipeline. D and K represent the dimension of the convolutional layers. In this study, D is equal to the output dimension of the SimCLR-. K is 16 for $D = 2, 4, 8$ & 64 for $D = 16, 32$, and 256 for $D = 64$.

Supplementary References

1. Wong, A., Wang, X. Y. & Hryniowski, A. *How much can we really trust you? Towards simple, interpretable trust quantification metrics for deep neural networks*. arXiv (2020) doi:10.48550/arXiv.2009.05835.
2. Hryniowski, A., Wong, A. & Wang, X. Y. Where Does Trust Break Down? A Quantitative Trust Analysis of Deep Neural Networks via Trust Matrix and Conditional Trust Densities. *Journal of Computational Vision and Imaging Systems* **6**, 1–5 (2021).
3. Triantafillou, E. *et al.* Meta-dataset: A dataset of datasets for learning to learn from few examples. (2020) doi:10.48550/arXiv.1903.03096.
4. Finn, C., Abbeel, P. & Levine, S. Model-agnostic meta-learning for fast adaptation of deep networks. in *34th International Conference on Machine Learning (ICML)* vol. 3 1856–1868 (PMLR, 2017).
5. Snell, J., Swersky, K. & Zemel, R. Prototypical networks for few-shot learning. in *Advances in Neural Information Processing Systems 30 (NeurIPS)* 4078–4088 (NeurIPS Proceedings, 2017).
6. He, K., Zhang, X., Ren, S. & Sun, J. Deep Residual Learning for Image Recognition. in *Proceedings of the IEEE Computer Society Conference on Computer Vision and Pattern Recognition (CVPR)* 770–778 (IEEE, 2006). doi:10.1109/CVPR.2006.200650130.
7. Fei-Fei, L., Deng, J. & Li, K. ImageNet: Constructing a large-scale image database. *J Vis* **9**, 1037–1037 (2010).
8. Chen, T., Kornblith, S., Norouzi, M. & Hinton, G. E. A simple framework for contrastive learning of visual representations. in *Proceedings of the 37th International Conference on Machine Learning (ICML)* 1597–1607 (PMLR, 2020).
9. Barz, B. & Denzler, J. Deep learning on small datasets without pre-training using cosine loss. in *Proceedings - 2020 IEEE Winter Conference on Applications of Computer Vision (WACV)* 1360–1369 (IEEE, 2020). doi:10.1109/WACV45572.2020.9093286.

Arxiv Logs:

1. Several grammatical errors or inconsistencies were addressed.
2. Language was significantly improved for fluidity and conciseness.
3. Figure 4 was edited to visually capture the differences between tasks.
4. The color palette of Tables 1 and 2 were simplified for better representation.
5. The presentation order was changed from “Introduction → Results → Discussion → Methods” to “Introduction → Methods → Results → Discussion → Conclusion” for better flow.